ChemComm

Atomic-scale Origin of the Enantiospecific Decomposition of Tartaric Acid on Chiral Copper Surfaces

Journal:	*ChemComm*
Manuscript ID	CC-COM-05-2024-002384.R1
Article Type:	Communication

The following section has been added to the manuscript:

Data availability

The data supporting this article have been included as part of the Supplementary Information

ChemComm

COMMUNICATION

Atomic-scale Origin of the Enantiospecific Decomposition of Tartaric Acid on Chiral Copper Surfaces

Received 00th January 20xx,
Accepted 00th January 20xx

DOI: 10.1039/x0xx00000x

Avery S. Daniels,[a] Andrew J. Gellman [b,c] and E. Charles H. Sykes*[a]

The origin of the enantiospecific decomposition of L- and D-tartaric acid on chiral Cu surfaces is elucidated on a structure-spread domed Cu(110) crystal by spatially resolved XPS and atomic-scale STM imaging. Extensive enantiospecific surface restructuring leads to the formation of surfaces vicinal to Cu(14,17,2) which are responsible for the enantiospecificity.

Structure-sensitive surface chemistry has been of longstanding interest in the fields of surface science and catalysis since the discovery that many surface reactions are sensitive to the structure of the surface.[1,2] The enantiospecific chemistry of chiral molecules on intrinsically chiral metal surfaces is a quintessential form of structure sensitive surface chemistry.[3] Enantiospecific differences in surface reaction kinetics arise solely from the lack of structural mirror symmetry of the chiral molecules and chiral surfaces. Therefore, building structure-function relationships for enantioselective reactions on chiral surfaces should provide valuable insight into the design of enantioselective heterogeneous catalysts, important for pharmaceutical, agrochemical, and other industries.[4-6]

In order to determine whether or not a surface chemical reaction is structure-sensitive, experiments on a number of surface orientations must be performed in order to probe orientation specific differences in reaction kinetics. The unambiguous observation of surface structure sensitivity was arguably the first major contribution of the field of surface science to the field of catalysis.[7] However, traditional experimental design has utilized single crystals that expose only a single facet or surface orientation making the comprehensive study of surface structure sensitivity across surface orientation space intractable.[8,9] To circumvent this issue, surface structure spread single crystals (S^4Cs) have been designed to expose a continuous distribution of surface orientations on a single sample (Figure 1A). On spherical S^4Cs, the vast majority of these orientations are chiral, and therefore, the use of spherical S^4Cs provides a high-throughput method for determining the optimum surface structure for enantiospecific reactions of chiral adsorbates.[10-12] Specific to this work, tartaric acid (TA) decomposition on chiral Cu surfaces is known to be highly enantiospecific, but the atomic scale origin of this effect is unknown.

To study the enantiospecific decomposition of L- and D-TA on chiral Cu surfaces, we utilized a novel Cu(110) S^4C with a domed-shape (Figure 1) that exposes a continuous array of chiral Cu facets on a single sample, as described in detail in our previous publications.[13-15] The reactivity of D-TA on the S^4C was previously measured utilizing spatially resolved X-ray photoelectron spectroscopy (XPS).[10] When combined with scanning tunneling microscopy (STM) images from various points on the Cu(110) S^4C, these studies reveal how Cu surface reconstruction, in the form of step bunching, occurs at the most enantiospecific regions of the sample surface orientation.

Figure 1 shows a photograph of the Cu(110) S^4C which was first imaged by STM at multiple locations to verify that the measured step densities and surface orientations corresponded to that expected for the domed-shape. The insets in Figure 1A show how the monoatomic step edges located 1.25 mm from the S^4C pole also follow the macroscopic curve of the sample. An atomic resolution STM image of the (110) pole is also shown. Full Cu(110) S^4C characterization data are summarized in Figure S.I.1.

In terms of chirality, the Cu(110) ± 14° S^4C exposes four quadrants separated by high-symmetry directions aligned with the Cu surface lattice. The top right and bottom left quadrants expose surfaces of S chirality, and the top left and bottom right quadrants expose surfaces of R chirality as seen in Figure 1B. Reflecting a quadrant through the vertical or horizontal mirror planes generates surfaces with the same surface structure, but opposite chirality. These surfaces interact enantiospecifically with chiral molecules altering their reactivity as demonstrated by the spatially resolved XPS map of the C1s signal during isothermal heating of the TA covered Cu(110) ± 14° S^4C at 433 K shown in Figure 1B. It is obvious from this data that D-TA decomposition occurs faster on surfaces of S chirality than on R surfaces, and hence the decomposition of TA is enantiospecific. The half-life, $t_{1/2}$, of the TA decomposition reaction is a convenient descriptor to quantify the enantiospecificity, in that

[a] Department of Chemistry, Tufts University, Medford, MA 02155, USA. E-mail: charles.sykes@tufts.edu
[b] Department of Chemical Engineering, Carnegie Mellon University, Pittsburgh, PA 15123
[c] W.E. Scott Institute of Energy Innovation, Carnegie Mellon University, Pittsburgh, PA 15123

† Electronic Supplementary Information (ESI) available: Experimental methods and additional data. See DOI: 10.1039/x0xx00000x

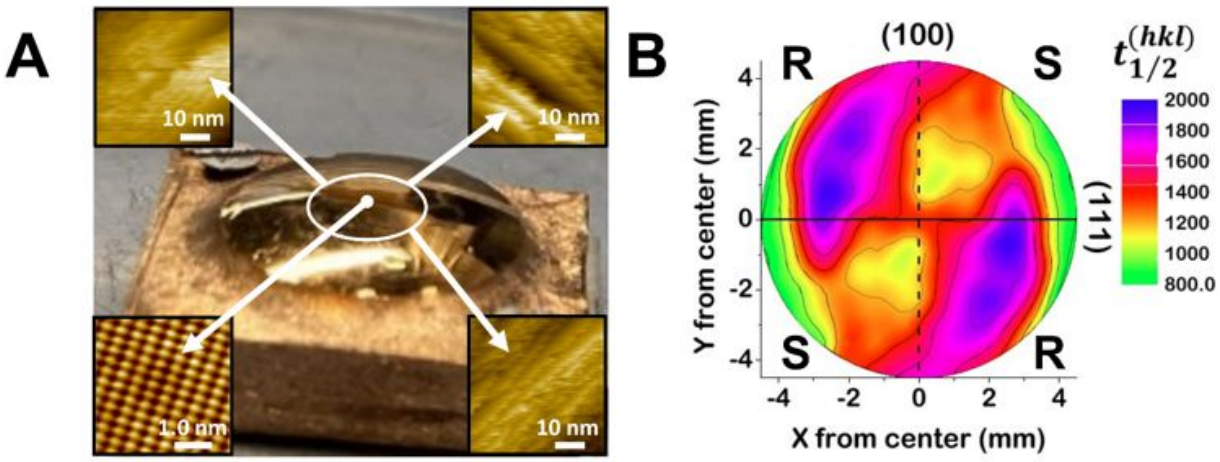

Figure 1: A) Photograph of the Cu(110) ± 14° S⁴C showing the domed surface. The insets are STM images showing how the step edge orientation depends on location on the S⁴C, and atomic resolution of the (110) pole. B) Schematic indicating the chirality of the different regions and the half-life of D-TA decomposition at various locations on the Cu(110) S⁴C derived from. The dashed line and solid line are high symmetry directions in achiral regions which contain step edges of (100) and (111) orientations, respectively. D-TA reacts away more slowly on Cu facets of R chirality than S chirality. Panel B adapted with permission from *Langmuir,* 2019, **35**, 16438–16443. *Copyright © 2019 American Chemical Society.*

$t_{1/2}$ is an observable easily obtainable from the time-dependent XPS maps. Specifically, to quantify the enantiospecificity, the difference in $t_{1/2}$ between points on the S⁴C reflected through the vertical mirror plane was used, and any facet with $|\Delta t_{1/2}| >$ 550s was considered to be highly enantiospecific. A second descriptor was derived from the free energies of activation, ΔG_{act}, where again the difference in ΔG_{act} was calculated from points reflected through the vertical mirror plane. Any facet with $|\Delta\Delta G_{act}| >$ 2.5 kJ/mol was considered a facet with high enantiospecificity. Unsurprisingly, similar regions of high enantiospecificity were found for the two different descriptors. Together, these descriptors demonstrate that the Cu(14,17,2) facet and those vicinal to it are the most enantiospecific to TA decomposition, as these facets have the largest $|\Delta t_{1/2}|$ and $|\Delta\Delta G_{act}|$, as indicated by the white crosses in Figure 2G.

STM was then used to investigate the atomic-scale surface structure at the points of high enantiospecificity, as found by XPS mapping on the Cu(110) S⁴C and shown in Figure 2. All STM

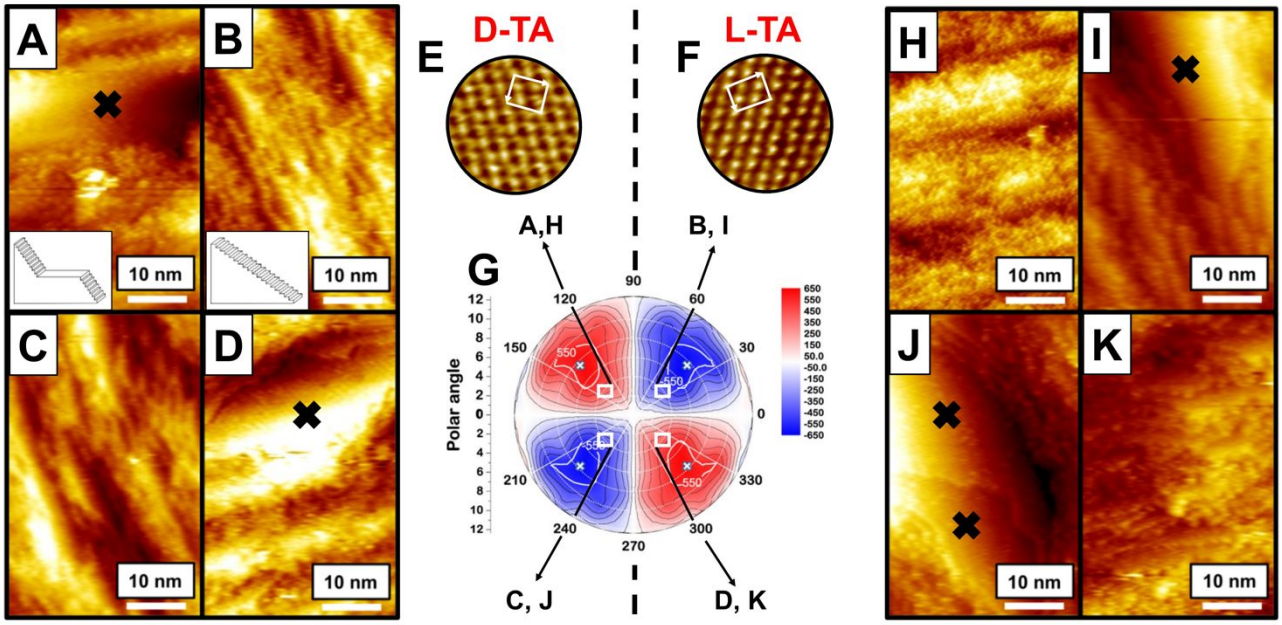

Figure 2: Representative STM images of D- and L-tartaric acid overlayers on the Cu(110) S⁴C at different spatial locations. The black X symbols on the STM images indicate the large terraces formed as a consequence of step bunching. A & D) STM images of the D-TA overlayer on surface facets of R chirality where step bunching occurs leading to the growth of large terraces. B & C) STM images of the D-TA overlayer on surface facets of S chirality where the step density is homogenous. E & F) Molecular resolution STM images of the D- and L-TA overlayer, respectively at the center of the Cu(110) S⁴C. G) Map of TA decomposition $\Delta t_{1/2}$ across the S⁴C. White contour lines enclose regions of high enantiospecificity. White squares indicate the regions of the S⁴C where STM images were acquired with arrows pointing to the letter corresponding to the panel. H-K) STM images of the opposite enantiomer of TA (L) where it can be seen that the step bunching is spatially mirrored. The dashed line in the center of the figure represents the spatial symmetry of the unit cell and step bunching based upon the enantiomer dosed on the S⁴C. Panel G adapted with permission from *Langmuir,* 2019, **35**, 16438–16443. *Copyright © 2019 American Chemical Society*.

images were acquired at 1.5 mm from the center (110) pole of the S[4]C sample unless otherwise specified. The measured unit cell dimensions, shown in Figure 2E for a saturated monolayer of D-TA at the center of the Cu(110) S[4]C, where the flat Cu(110) facet is present, are 1.46 ± 0.05 nm x 1.06 ± 0.06 nm and the close-packed direction of the D-TA overlayer is rotated 19.2 ± 1.9° clockwise from the close-packed of the underlying Cu(110) lattice. Similarly, Figure 2F shows the unit cell for L-TA at the center of the Cu(110) S[4]C with measurements: 1.51 ± 0.04 nm x 1.07 ± 0.04 nm with the close-packed direction of the overlayer rotated 21.4° ± 3.2 counterclockwise from the close-packed direction of Cu(110). These measurements indicate that 5 TA molecules occupy the area of 18 surface Cu atoms, giving a density of 0.28 TA molecules per Cu atom for both L- and D-TA, in agreement with previous studies of saturated monolayers of TA on a flat Cu(110) single crystal.[16-19] Given that the TA unit cells are rotated away from the high-symmetry directions of the Cu surface, the surface-bound TA overlayers are themselves chiral in addition to the intrinsic chirality of the molecules. Additionally, this well-ordered TA overlayer persists away from the center (110) pole in the more stepped and enantiospecific regions of the sample as seen in Figure S.I. 2C.

When comparing the different quadrants in Figure 2 A-D and H-K, it is obvious that during TA decomposition, significant surface restructuring occurs, and that it is enantiospecific. Specifically, for D-TA adsorption, the STM images in Figure 2A-D indicate that on surfaces of R chirality, restructuring of the surface occurs leading to the formation of terraces larger than 10 nm surrounded by much smaller <1 nm wide terraces. In contrast, surfaces of S chirality have a more homogenous terrace width ~ 1.2 nm (or equivalently, more homogenous step edge density) and no terraces larger than 10 nm. Control experiments with L-TA on the same Cu S[4]C sample shown in Figure 2H-K produced mirror image results, confirming that the origin of the effect arises from enantiospecific molecule-surface interactions, and not for example, defects in certain areas of the Cu S[4]C sample.[14] Therefore, the observed reconstruction of the surface is enantiospecific and depends both on the enantiomer bound to the surface, and the chirality of the surface itself. For the surface chirality and enantiomer combinations where step bunching occurs, terraces wider than 10 nm are produced in order to keep the overall step density consistent with that imposed by the dome-shaped nature of the S[4]C.

Further corroboration that the observed step bunching is due to diastereomerism in the TA-Cu surface interaction ($R_{surf}L_{TA}$ vs $S_{surf}L_{TA}$) can be seen in the STM data in Figure 3, which quantify the terrace width distribution for L-TA on R and S chirality surfaces. For L-TA, we examined regions 1.5 mm from the center of the crystal (Figure 3A & B) as images at 2.0 mm from the pole (Figure S.I. 2A) showed the same step bunching effect, we therefore acquired and analyzed data at 1.5 mm from the pole due to difficulty of STM image acquisition in highly stepped regions. A total of ~100 terrace widths were measured for each surface chirality perpendicular to the direction of the step edges. Figure 3A shows the terrace width distribution for R chirality surfaces, where no step bunching occurred, while Figure 3B shows the terrace width distribution for S chirality surfaces where step bunching occurred. We found that where step bunching occurred there were 23 terrace widths of 0.9 ± 0.15 nm while the region with no step bunching had only 11 terrace widths of 0.9 ± 0.15 nm and the expected terrace width for the Cu(14,17,2) facet is 0.97 nm wide.

It can also be seen in Figure 3 that the S chirality surfaces have several very large terraces while the R chirality surfaces do not. Specifically, for R chirality surfaces, there are only 2 terraces with width greater than 5 nm, neither of which are greater than 10 nm. However, on S chirality surfaces, 4 terraces were measured with width greater than 10 nm. Interestingly, the average terrace width wider than 5 nm for R chirality surfaces was 7.9 ± 0.9 nm while for S chirality surfaces it was

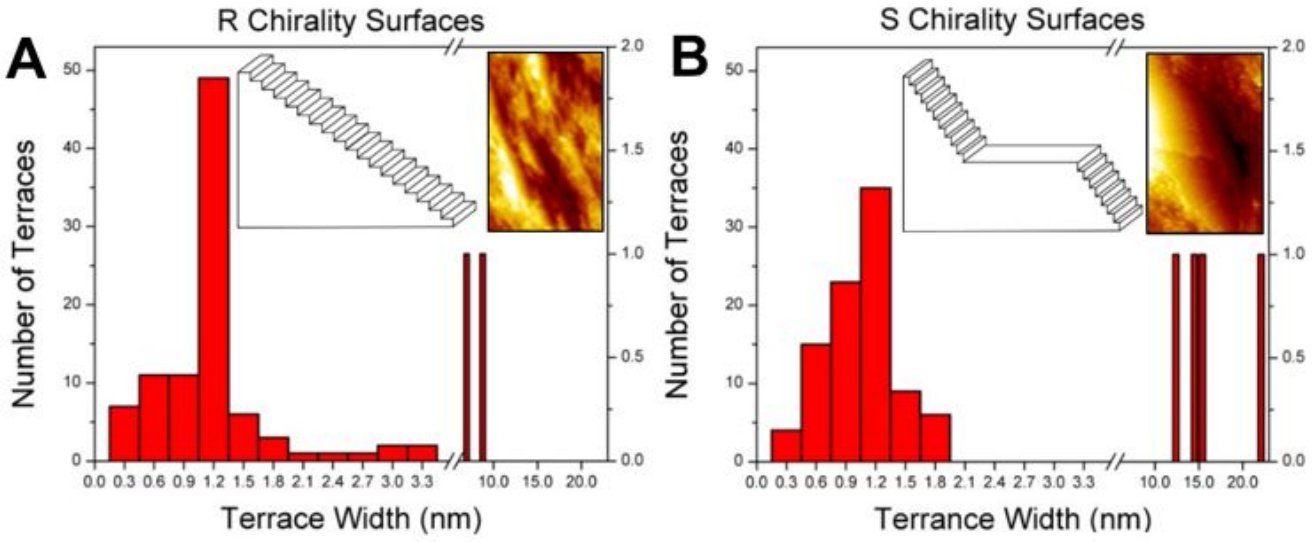

Figure 3: Quantitative analysis of the step bunching induced by adsorption of L-TA in areas of R and S chirality on the Cu(110) S[4]C. A) Terrace width distribution on R chirality surfaces. The maximum measured terrace width was 8.75 nm. Inset shows a representative STM image of L-TA on the R surface and schematic of the homogenous step density. B) Terrace width distribution on S chirality surfaces. The maximum measured terrace width was 22.1 nm. Inset is a representative STM image of L-TA on the S surface and schematic of the heterogenous step density caused by step bunching.

16.1 ± 3.6 nm. Together, these experimental results demonstrate that TA adsorption on 110 terminated Cu surfaces leads to enantiospecific restructuring of the surface in the form of step bunching, which in turn gives rise to enantiospecific TA decomposition kinetics.

The fact that the step bunching occurs spontaneously, and the bare Cu surface does not restructure in this way (see S.I. Figure S.I.1), infers that the formation of stronger Cu-TA bonds at the restructured interface must drive the restructuring process itself. We therefore hypothesize that step bunching occurs to make the preferred Cu(14,17,2) facet or a facet with similar step and kink density to that of Cu(14,17,2), driven by the strong bonding of L-TA to Cu surfaces of S chirality or D-TA to Cu surfaces of R chirality. This is illustrated by the step density schematics in Figure 2 A & B and Figure 3 A & B where D-TA and L-TA restructure R and S chirality surfaces, respectively and don't restructure S and R surfaces, respectively. Moreover, the region of high enantiospecificity in Figure 2G is large which is consistent with our findings that areas even 1.5 mm from the center of the sample restructure to yield locally Cu(14,17,2)-like facets, interspersed by the occasional wide terrace. Furthermore, these stronger TA-Cu bonds in the most enantiospecific regions of the sample lead to the slowest TA decomposition kinetics and hence the longest $t_{1/2}$. Most interestingly, this effect is enantiospecific with D-TA restructuring R chirality surfaces and L-TA restructuring S chirality surfaces with the most pronounced effect at a radius of ~2.75 mm from the center pole corresponding to Cu(14,17,2) and vicinal facets[10] as seen in Figure 1B.

Combining spatially resolved XPS data of TA decomposition and STM imaging of the enantiospecific surface restructuring enabled us to propose an atomic-scale mechanism behind the observed macroscopic enantiospecific TA decomposition kinetics on chiral Cu surfaces. The Cu(110) ± 14° S^4C sample enabled mapping of the decomposition kinetics of D-TA on ~1/3 of all of structure space, revealing highly enantiospecific regions. Atomic-scale imaging of L- and D-TA in enantiospecific regions revealed that, depending on the chirality of the molecule and the surface facet, large-scale restructuring of the Cu surface was observed in the form of step bunching. This step bunching was driven by the formation of regions of Cu(14,17,2) or similar facets which bind the correct enantiomer of TA more strongly than the unreconstructed surface. This spontaneous surface restructuring which enables stronger Cu-TA interactions leads to slower TA decomposition kinetics. For the same enantiomer of TA, regions of opposite surface chirality do not exhibit this restructuring, leading to highly enantiospecific decomposition of TA thereby shedding light on the nanoscale surface restructuring that leads to highly enantioselective TA decomposition kinetics. This study also highlights the utility of S^4Cs in enabling high-throughput investigation of chiral surface structure, restructuring, and the reactivity of a vast number of local surface facets on a single sample.

Conflicts of interest

There are no conflicts to declare.

Data availability

The data supporting this article have been included as part of the Supplementary Information.

Notes and references

1 G. Ertl, *Angew. Chem., Int. Ed.,* 2008, **47**, 3524−3535
2 F. Zaera, A.J. Gellman, and G.A. Somorjai, *Acc. Chem. Res.,* 1986, **19**, 24–31.
3 A.J. Gellman, *Acc. Mater. Res.,* 2021, **2**, 1024-1032.
4 G. Kyriakou, S. K. Beaumont, and R. M. Lambert, *Langmuir,* 2011, **27**, 9687−9695.
5 L. A. Nguyen, H. He, and C. Pham-Huy, *Int. J. Biomed. Sci.,* 2006, **2**, 85– 100
6 R. Noyori, *Angew. Chem., Int. Ed.,* 2002, **41**, 2008−2022.
7 F. Bozso, G. Ertl, and M. Weiss, *J. Catal.,* 1977, **50**, 519–529.
8 A.J. Gellman, Y. Huang, A.J. Koritnik, and J.D. Horvath, *J. Phys. Condens. Matter*, 2016, **29**, 034001.
9 S.J. Jenkins and S.J. Pratt, *Surface Science Reports*, 2007, **62**, 373-429.
10 B. Karagoz, M. Payne, A. Reinicker, P. Kondratyuk, and A.J. Gellman, *Langmuir,* 2019, **35**, 16438–16443.
11 C. Fernández-Cabán and A.J. Gellman, *J. Phys. Chem. C,* 2021, **125**, 9766–9773.
12 C. Fernández-Cabán, B. Karagoz, P. Kondratyuk, and A.J. Gellman, *Mater. Adv.*, 2022, **3**, 2191-2199.
13 A. de Alwis, B. Holsclaw, V.V. Pushkarev, A. Reinicker, T.J. Lawton, M.E. Blecher, E.C.H. Sykes, and A.J. Gellman, *Surface Science*, 2013, **608**, 80-87.
14 A.C. Schilling, A.J. Therrien, R.T. Hannagan, M.D., Marcinkowski, P.L. Kress, D.A. Patel, T.A. Balema, A.M. Larson, F.R. Lucci, B.P. Coughlin, R. Zhang, T. Thuening, V. Çinar, J. McEwen, A.J. Gellman, and E.C.H. Sykes, *ACS Nano*, 2020, **14**, 4682-4688.
15 A.D. Reinicker, A.J. Therrien, T.J. Lawton, R. Ali, E.C.H. Sykes, and A.J. Gellman, *Chem. Commun.*, 2016, **52**, 11263-11266.
16 M. O. Lorenzo, V. Humblot, P. Murray, C. J. Baddeley, S. Haq, and R. Raval, *J. Catal.*, 2002, **205**, 123−134.
17 B. Behzadi, S. Romer, R. Fasel, and K. H. Ernst, *J. Am. Chem. Soc.* 2004, **126**, 9176−9177A.
18 M. O. Lorenzo, S. Haq, T. Bertrams, P. Murray, R. Raval, and C.J. Baddeley, *J. Phys. Chem. B,* 1999, **103**, 10661−10669.
19 B.S. Mhatre, V. Pushkarev, B. Holsclaw, T.J. Lawton, E.C.H. Sykes, and A.J. Gellman, J*. Phys. Chem. C*, 2013, **117**, 7577−7588.